Vortex solitons in defocusing media with spatially inhomogeneous nonlinearity

Qing Tian, Lei Wu, Yonghao Zhang, and Jie-Fang Zhang

Phys. Rev. E **85**, 056603 — Published 11 May 2012

DOI: 10.1103/PhysRevE.85.056603

Vortex solitons in defocusing media with spatially inhomogeneous nonlinearity

Qing Tian,[1,2] Lei Wu,[2] Yonghao Zhang,[2] and Jie-Fang Zhang[3,1]

[1]*School of Physics Science and Technology, Soochow University, Suzhou, Jiangsu 215006, P. R. China*
[2]*Department of Mechanical and Aerospace Engineering, University of Strathclyde, Glasgow, G1 1XJ, UK*
[3]*Zhejiang University of Media and Communications, Hangzhou 310018, Zhejiang, China*

The analytical two- and three-dimensional vortex solitons with arbitrary values of vorticity are constructed in the cubic defocusing media with spatially inhomogeneous nonlinearity. The values of the nonlinearity coefficients are zero near the center and increase rapidly toward the periphery. In addition to the analytical ones, a number of vortex solitons are found numerically. It is shown that analytical vortex solitons are stable. Also, the stability region of the numerically constructed vortex solitons are given.

PACS numbers: 05.45.Yv, 42.65.Tg, 03.75.Lm

I. INTRODUCTION

The nonlinear Schrödinger equation (NLSE) is a ubiquitous equation that has important applications in nonlinear optics [1], Bose-Einstein condensations (BECs) [2], and fluid dynamics. It gives rise to solitons when the nonlinearity and dispersion/diffraction are balanced. The investigation of soliton solutions will help us to improve the signal transmission capacity in nonlinear optical fibers, to understand the ultracold gas dynamics in BECs, and to explain the formation and decay of rogue waves in oceans [3]. Due to the experimental controllability of system parameters such as the nonlinearity, dispersion, gain, and external potential, intensive efforts have been devoted to constructing analytical soliton solutions.

The standard one-dimensional (1D) NLSE supports analytical bright and dark solitons when the cubic nonlinearities are self-focusing and self-defocusing, respectively. By means of the self-similar transformation, these analytical solitons can also be found in nonautonomous NLSE when the magnitudes of system parameters vary with the propagation variable in delicate ways [4–7]. Unlike the standard NLSE solitons, the amplitude, width, center-of-mass, and frequency chirp of the nonautonomous solitons can be manipulated by demand, offering the opportunity for light guiding and compression.

Analytical solitons can also be constructed in 1D and 2D NLSEs by the canonical transformations [8–12] when the nonlinearity varies with the transverse variable [13]. Thus far, it is found that the localized solitons, whose intensities go to zero at the tails, exist only in the presence of external potential (such as the periodic and harmonic potentials) when the nonlinearity is self-defocusing. Another approach to finding the analytical solitons relies on the use of the inverse problem [14]. Recently, it is reported that the defocusing spatially inhomogeneous nonlinearity (DSIN) can support analytical localized solitons in all three dimensions, as long as the DSIN strength increases rapidly enough toward the periphery [15].

Despite the analytical progress, it is still challenging to find the stable vortex solitons with high values of vorticity S in the 3D NLSE. In the numerical studies, 3D stable vortex solitons with $S = 1$ and $|S| \leq 2$ have been found in the conservative NLSE with a competing nonlinearity [16] and the dissipative NLSE [17], respectively.

Here we construct the analytical vortex solitons with arbitrary values of integer vorticity in 2D and 3D NLSEs when the DSIN strength increases rapidly enough from the center to the periphery. We adopt this kind of DSIN because it supports 2D stable vortex solitons with high values of vorticity [15]. Our results will yield the first example of stable vortex solitons with higher vorticities in the 3D conservative NLSE with the cubic nonlinearity,

$$i\psi_\xi = -\nabla^2\psi + V\psi + g|\psi|^2\psi. \tag{1}$$

In nonlinear spatial optics, ψ is the amplitude of electromagnetic field, ξ is the propagation variable, V is the local refractive index, and the spatially-dependent nonlinearity coefficient g can be achieved by the nonuniform distribution of nonlinearity-enhancing dopants [18]. In BECs, ψ is the wave function, ξ stands for the time, V is the external potential, and g is related to the s-wave scattering length which can be controlled via the Feshbach resonance [19–21].

II. THE 2D VORTEX SOLITON SOLUTIONS

We first construct the 2D analytical vortex soliton solutions in the absence of external potential. They are searched in the form of

$$\psi(r, \theta, \xi) = \phi(r) \exp(iS\theta - i\mu\xi), \tag{2}$$

where r is the radial coordinate, θ is the azimuthal angle, $\mu > 0$ is the soliton eigenvalue, S (integer) is the vorticity, and the real function $\phi(r)$ describes the amplitude profile of the vortex soliton which satisfies

$$\mu\phi = -\phi_{rr} - \frac{1}{r}\phi_r + \frac{S^2}{r^2}\phi + g(r)\phi^3. \tag{3}$$

Note that at the vortex core $r \to 0$, if the strength of DSIN does not diverge, the asymptotic behavior of the amplitude profile is $\phi(r) \sim r^{|S|}$.

In order to construct the analytical vortex solitons, we introduce the canonical transformation [11]

$$\phi(r) = \rho(r)U[R(r)], \quad R(r) = \int_0^r \eta^{-1}\rho(\eta)^{-2}d\eta, \tag{4}$$

to Eq. (3), and find $U[R(r)]$ satisfies the following ordinary differential equation

$$EU = -U_{RR} + g(r)\rho^6(r)r^2U^3, \tag{5}$$

where $E = \rho^3 r^2\left[\rho_{rr} + \rho_r/r + \left(\mu - S^2/r^2\right)\rho\right]$.

Assume that $\rho(r) = f(r)/\sqrt{r}$, one finds that $f(r)$ satisfies the Ermakov-Pinney equation [8]: $f_{rr} + [\mu - (4S^2 - 1)/4r^2]f = Ef^{-3}$. To get the analytical solution for $f(r)$, let E be a constant. Then we have

$$\rho(r) = \sqrt{\alpha J^2 + 2\beta JY + \gamma Y^2}, \tag{6}$$

where $J(S, \sqrt{\mu}r)$ and $Y(S, \sqrt{\mu}r)$ are the Bessel functions of the first and second kinds, respectively. The constants α, γ, and $E = 4(\alpha\gamma - \beta^2)/\pi^2$ are positive, ensuring that $\rho(r)$ is real and $\rho(r) \neq 0$.

The requirements for $U(R)$ can be analyzed as follows. At $r \to 0$, we have $\rho(r) \sim r^{-|S|}$ and $R(r) \sim r^{2|S|}$. Since $\phi(r) \sim r^{|S|}$, $U(R)$ should vary as R when $R \to 0$. Meanwhile, at $r \to \infty$, we find $\rho(r) \sim (\sqrt{\mu}r)^{-1/2}$ and $R(r)$ increases linearly as r grows. Therefore, $U(R \to \infty) \to 0$ is required. The two asymptotic conditions for $U(R)$ can be realized when the nonlinearity profile is

$$g(r) = \frac{\widetilde{V}(R)}{\rho^6(r)r^2U^2[R(r)]}, \tag{7}$$

and $U(R)$ is the first-excited-state solution of the linear Schrödinger equation with the effective potential $\widetilde{V}(R)$:

$$EU = -U_{RR} + \widetilde{V}(R)U. \tag{8}$$

The virtue of the above transformation is that one can utilize the abundant solutions of the linear Schrödinger equation to construct the analytical vortex soliton solutions. For example, let $\widetilde{V}(R) = E^2R^2/9$ be the harmonic potential, the first-excited-state solution of Eq. (8) is

$$U[R(r)] = R(r)\exp\left[-\frac{E}{6}R(r)^2\right], \tag{9}$$

and the corresponding nonlinearity profile is

$$g(r) = \frac{E^2}{9\rho^6(r)r^2}\exp\left[\frac{E}{3}R(r)^2\right]. \tag{10}$$

We can also let $\widetilde{V}(R) = 6E\tanh^2(\sqrt{E/5}R)/5$, then the first-excited-state solution of Eq. (8) is

$$U[R(r)] = \tanh\left[\sqrt{\frac{E}{5}}R(r)\right]\mathrm{sech}\left[\sqrt{\frac{E}{5}}R(r)\right], \tag{11}$$

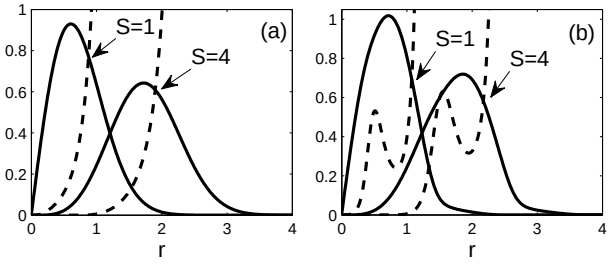

FIG. 1: Amplitude profiles $\phi(r)$ of the 2D analytical vortex solitons (solid lines) and the corresponding nonlinearity landscapes $g(r)$ (dashed lines, normalized by 10). Solutions are given by Eqs. (4), (6), (9), and (10). Parameters are $\mu = 10$, $\alpha = \gamma = 1$, and $\beta = 0$ in (a) and $\beta = 0.5$ in (b).

and the corresponding nonlinearity profile is

$$g(r) = \frac{6E}{5\rho^6(r)r^2\,\mathrm{sech}^2[\sqrt{E/5}R(r)]}. \tag{12}$$

It follows from Eqs. (10) and (12) that the nonlinearity strength at $r \to 0$ is determined by the vorticity, i.e., $g(r) \sim r^{6|S|-2}$, while at $r \to \infty$ it is determined by the soliton eigenvalue and the solution (9) or (11). For the given solution, the larger the soliton eigenvalue, the faster the nonlinearity strength approaches infinity. For the given soliton eigenvalue, the nonlinearity strength given by Eq. (10) grows faster than that of Eq. (12). In the intermediate region, $g(r)$ increases monotonically when $\alpha = \gamma$ and $\beta = 0$, while when $\alpha \neq \gamma$ or $\beta \neq 0$, there could be some oscillations in the nonlinearity profile. Typical amplitude profiles of analytical vortex solitons and the corresponding nonlinearity landscapes $g(r)$ are depicted in Fig. 1.

To elucidate the stability of the analytical vortex solitons, we substitute a perturbed solution

$$\begin{aligned}\psi(r,\theta,\xi) =&[\phi(r) + u(r)\exp(i\delta\xi + iM\theta) + \\ &v^*(r)\exp(-i\delta^*\xi - iM\theta)]\exp(iS\theta - i\mu\xi)\end{aligned}$$

with azimuthal perturbation index M into Eq. (1) and solve the following linearized eigenvalue problem:

$$\delta u = \left[\frac{d^2}{dr^2} + \frac{1}{r}\frac{d}{dr} - \frac{(S+M)^2}{r^2} + \mu - 2g\phi^2\right]u - g\phi^2 v,$$
$$\delta v = -\left[\frac{d^2}{dr^2} + \frac{1}{r}\frac{d}{dr} - \frac{(S-M)^2}{r^2} + \mu - 2g\phi^2\right]v + g\phi^2 u.$$

We have calculated the eigenvalue δ using the vortex soliton solution (9) and (10) when $\mu = 10$, $\alpha = \gamma = 1$, $\beta = 0$ (or 0.5), and vorticity $S = 1, 2, \cdots, 100$. The numerical results show that all the eigenvalues δ are real, which indicates all the analytical vortex solitons are linearly stable.

Note that the analytical vortex solutions exist for positive soliton eigenvalue μ, and one particular nonlinearity profile $g(r)$ supports only one analytical vortex soliton in general. However, for a given nonlinearity profile $g(r)$

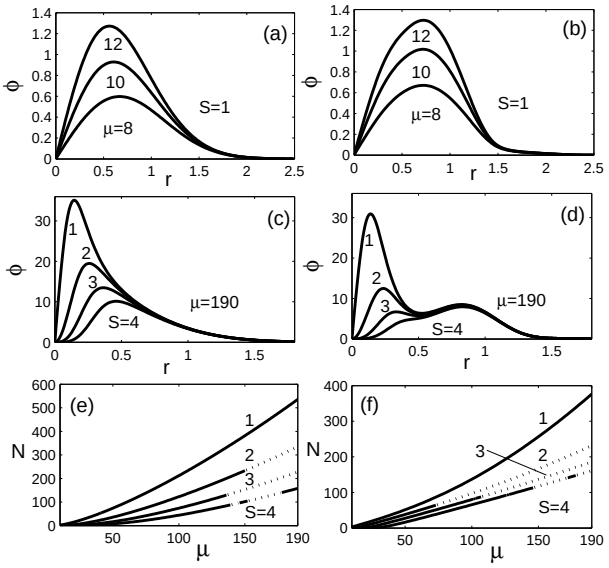

FIG. 2: (a-d) Amplitude profiles of the 2D numerically constructed vortex solitons. (e, f) Soliton norm N vs soliton eigenvalue μ. Solid and dotted lines stand for stable and unstable solitons. The nonlinearity $g(r)$ in left and right columns are depicted in Fig. 1(a) and Fig. 1(b) when $S = 1$, respectively.

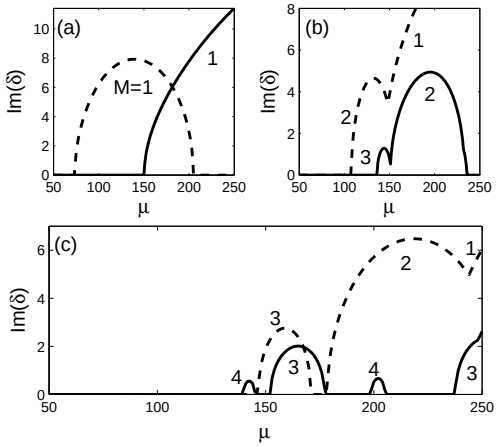

FIG. 3: Imaginary parts of the eigenvalue δ for vortex solitons with (a) $S = 2$, (b) $S = 3$, and (c) $S = 4$. The numbers near the lines are the azimuthal perturbation index M where the vortex solitons are mostly unstable. The nonlinearity profiles $g(r)$ for the solid and dashed lines are depicted in Fig. 1(a) and Fig. 1(b) when $S = 1$. Vortex solitons with $0 < \mu < 50$ are all stable.

that supports the analytical vortex soliton with particular values of μ and S, there are other vortex solitons with different values of μ and S. The later can be constructed numerically by the relaxation method.

The numerical results are summarized in Fig. 2. The numerically constructed vortex soliton families are characterized by the soliton norm $N = 2\pi \int r\phi^2 dr$ and the integer vorticity S. For fixed vorticity S, the increase of soliton eigenvalue μ results in the increase of the soliton's amplitude and norm. For fixed soliton eigenvalue, the increase of vorticity yields the decrease of the soliton's amplitude and norm; although vortex solitons with different values of vorticities have different asymptotic amplitude profiles at $r \to 0$, i.e., $\phi(r) \sim r^S$, they share the same amplitude profile at $r \to \infty$. This asymptotic behavior can be explained by the Thomas-Fermi approximation: at $r \to \infty$, terms such as $\phi_{rr}, \phi_r/r, \phi/r^2$ in Eq. (3) are not important, so that $\phi(r) \approx \sqrt{\mu/g(r)}$ [22].

The linear stability of the numerically constructed vortex solitons can be analyzed by the same way with that for the analytical vortex solitons. The numerical results indicate that all the numerically constructed vortex solitons with $S = 1$ are stable, but the numerically constructed vortex solitons with $S \geq 2$ exhibit a pattern: switching between stable and unstable as μ increases. The switching pattern has also been observed in [15]. In Fig. 3 we plot the instability growth rate vs the soliton eigenvalue. We also show the perturbation index M under which the vortex solitons are most likely unstable. The switching pattern can be clearly seen in Fig .3(c). However, it is difficult to generalize how the switching pattern emerges, since the switching happens irregularly, that is, the size of the instability region and the intervals between two continuous instability regions are different.

Notice that the nonlinearity strength goes to infinity as r increases. In experiments, it would be impossible to have such rapid nonlinearity variations extending to large r; instead, the rapid variation would saturate at some point and $g(r)$ would become constant for $r > r_s$. In this case, one would expect the leak-away of the soliton energy. In numerical simulations we use the absorption boundary condition to mimic the energy-leaking. We find that when r_s is larger than the size of the vortex soliton (for example, $r_s = 3$ for vortex soliton with $S = 1$ in Fig. 1), the leak-away of the soliton energy is negligible. On the other hand, if r_s is too small, the localized vortex solitons do not exist because of the repulsive nonlinearity (the amplitude of the vortex soliton is a nonzero constant when $r \to \infty$).

It should also be noted that, although only the results when g is given by Eq. (10) is shown, similar conclusions hold when g is given by Eq. (12).

III. THE 3D VORTEX SOLITON SOLUTIONS

Next we construct the 3D analytical vortex soliton solutions in the presence of external potential in BECs. Experimentally, harmonic potentials are usually used to confine the condensates. For pancake-shaped BECs, the longitudinal trapping frequency ω is much larger than the transversal one. Hence the transversal harmonic potential is negligible. The 3D analytical vortex soliton solution is searched in the form of

$$\psi(r, \theta, z, \xi) = \phi(r, z) \exp(iS\theta - i\mu\xi), \qquad (13)$$

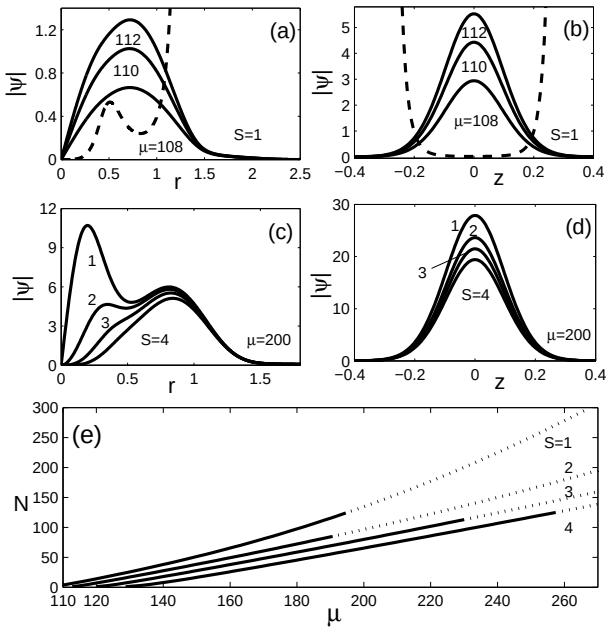

FIG. 4: (a-d) Cross-section shapes of 3D vortex solitons and nonlinearity landscapes (dashed lines, normalized by 10). (e) Soliton norm vs soliton eigenvalue μ. The solid and dotted lines stand for stable and unstable branches, respectively. Parameters are given in the text.

where r is the radial coordinate, θ is the azimuthal angle, z is the longitudinal spatial coordinate, ξ is time, and the amplitude profile ϕ (real function) satisfies $\mu\phi = -\phi_{rr} - r^{-1}\phi_r + S^2 r^{-2}\phi - \phi_{zz} + \omega^2 z^2\phi + g\phi^3$.

If the nonlinearity profile is separable in the transversal and longitudinal directions, i.e.,

$$g(r,z) = A^{-2} g_1(r)\exp(\omega z^2), \tag{14}$$

the 3D analytical vortex soliton solution can be given by

$$\phi(r,z) = A\phi_1(r)\exp\left(-\frac{\omega}{2}z^2\right), \tag{15}$$

where ϕ_1 obeys $(\mu-\omega)\phi_1 = -\phi_{1rr} - r^{-1}\phi_{1r} + S^2 r^{-2}\phi_1 + g_1(r)\phi_1^3$.

Following the above-mentioned process of constructing the 2D analytical vortex solitons, $\phi_1(r)$ can be exactly constructed, then one can find the 3D analytical vortex solitons. Typical cross-section amplitude profiles of the 3D analytical vortex solitons are shown in Fig. 4(a) and (b) when $S = 1$, $\mu = 110$, $\omega = 100$, $\alpha = \gamma = 1$, and $\beta = 0.5$. The nonlinearity profile in the radial direction $g_1(r)$ is the same as that in Fig. 1(b) when $S = 1$, while that in the longitudinal direction is $\sqrt{\pi/\omega}\exp(\omega z^2)$.

In addition to the analytical vortex soliton, the nonlinearity landscape used in Fig. 4 supports other vortex solitons with different values of μ and S. They can be found by substituting $\psi(r,\theta,z,\xi) = \widetilde{\phi}(r,z,\xi)\exp(iS\theta)$ into Eq. (1) and then solving the following equation numerically

$$i\widetilde{\phi}_\xi = -\widetilde{\phi}_{rr} - \frac{1}{r}\widetilde{\phi}_r + \frac{S^2}{r^2}\widetilde{\phi} - \widetilde{\phi}_{zz} + \omega^2 z^2\widetilde{\phi} + g|\widetilde{\phi}|^2\widetilde{\phi}. \tag{16}$$

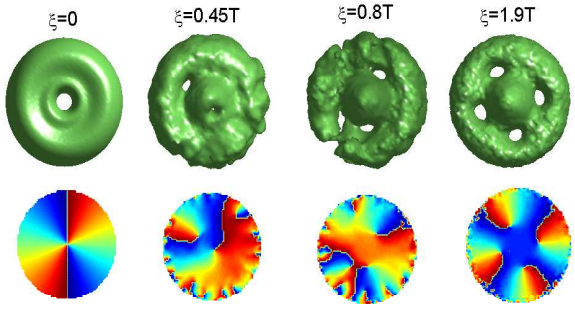

FIG. 5: (Color online) Evolution of the 3D vortex soliton with $S = 2$ at different propagation distances (here $T = 2\pi/\omega$). The first row shows the isosurface plot of the soliton amplitude at the value of 50, while the second row shows the phase structures at $z = 0$ plane. The soliton is initially perturbed by white noises with the perturbation amplitude at the 1% level, where the radial and longitudinal amplitude profiles of the numerically constructed vortex soliton are shown in Fig. 3(c) and (d).

Given the value of soliton norm $N = 2\pi\int rdr\int\widetilde{\phi}^2 dz$, the amplitude profile $\widetilde{\phi}$ can be solved by means of the imaginary-time method [23], and the corresponding soliton eigenvalue can be calculated by [24]

$$\mu = \frac{2\pi}{N}\int rdr\int\left[\widetilde{\phi}_r^2 + \widetilde{\phi}_z^2 + \left(\frac{S^2}{r^2} + \omega^2 z^2\right)\widetilde{\phi}^2 + g\widetilde{\phi}^4\right]dz.$$

The linear stability of the 3D vortex solitons is checked by inserting the perturbed solution

$$\begin{aligned}\psi(r,\theta,z,\xi) =& [\widetilde{\phi}(r,z) + u(r,z)\exp(i\delta\xi + iM\theta) + \\ & v^*(r,z)\exp(-i\delta^*\xi - iM\theta)]\exp(iS\theta - i\mu\xi)\end{aligned}$$

into Eq. (1) and solving the linearized eigenvalue problem. Since the 3D analytical vortex solitons use the 2D analytical vortex solitons as 'seeds', behavior of the 3D vortex solitons is similar as the 2D vortex solitons, except that the numerically constructed 3D vortex solitons with $S = 1$ are not all stable, see Fig. 4(e).

The stability analysis is also verified by direct simulations of Eq. (1). Typical unstable dynamics are shown in Fig. 5, where vortex soliton with $S = 2$ gradually decays into four vortex solitons with $S = 1$. For vortex solitons that were predicted to be linearly stable, they are indeed stable even when they are perturbed initially by white noises with the perturbation amplitude at the 20% level.

IV. CONCLUSIONS

In summary, analytical vortex solitons with arbitrary integer values of vorticity, including the 2D vortex solitons in the absence of external potential and 3D vortex solitons in the presence of harmonic potential, have been constructed in the NLSEs with the defocusing spatially inhomogeneous nonlinearity whose strength increases

rapidly toward the periphery. It has been found that the analytical 2D and 3D vortex solitons are all stable, and the numerically constructed ones with higher values of vorticity could also be stable. Note that the vortex solitons are constructed in the non-rotating frame. However, the combination of the methods in this paper and that in Ref. [25] could produce analytical vortex soliton solutions in the rotating frame. We believe the use of defocusing spatially inhomogeneous nonlinearity whose strength increases rapidly toward the periphery could yield stable vortex solitons with higher vorticity in the rotating frame. Also, this kind of defocusing nonlinearity may support more stable rotating azimuthal vortex clusters than that in the conventional NLSE with constant defocusing nonlinearity and harmonic potential [26].

This work has been supported by the National Natural Science Foundation of China under Grant No. 11072219 and 11005092.

[1] Y. S. Kivshar and G. P. Agrawal, *Optical Solitons: From Fibers to Photonic Crystals* (Academic Press, San Diego, 2003).

[2] L. Pitaevskii and S. Stringari, *Bose-Einstein Condensate* (Oxford University Press, Oxford, England, 2003).

[3] *Discussion and Debate: Rogue Waves–Towards a Unifying Concept?* Eur. Phys. J. Special Topics **185** (2010).

[4] V. N. Serkin and A. Hasegawa, Phys. Rev. Lett. **85**, 4502 (2000).

[5] V. I. Kruglov, A. C. Peacock, and J. D. Harvey, Phys. Rev. Lett. **90**, 113902 (2003).

[6] S. A. Ponomarenko and G. P. Agrawal, Phys. Rev. Lett. **97**, 013901 (2006).

[7] V. M. Pérez-García, P. J. Torres, V. V. Konotop, Physica D **221**, 31 (2006).

[8] J. Belmonte-Beitia, V. M. Pérez-García, and V. Vekslerchik, Phys. Rev. Lett. **98**, 064102 (2007).

[9] D. S. Wang, X. H. Hu, J. Hu, and W. M. Liu, Phys. Rev. A **81**, 025604 (2010).

[10] J. F. Zhang, Y. S. Li, J. Meng, L. Wu, and B. A. Malomed, Phys. Rev. A **82**, 033614 (2010).

[11] L. Wu, L. Li, J. F. Zhang, D. Mihalache, B. A. Malomed, and W. M. Liu, Phys. Rev. A **81**, 061805(R) (2010).

[12] Q. Tian, L. Wu, J. F. Zhang, B. A. Malomed, D. Mihalache, and W. M. Liu, Phys. Rev. E **83**, 016602 (2011).

[13] Y. V. Kartashov, B. A. Malomed, and L. Torner, Rev. Mod. Phys. **83**, 405 (2011).

[14] B. A. Malomed and Yu. A. Stepanyants, Chaos **20**, 013130 (2010).

[15] O. V. Borovkova, Y. V. Kartashow, L. Torner, and B. A. Malomed, Phys. Rev. E **84**, 035602(R) (2011).

[16] D. Mihalache, D. Mazilu, L.-C. Crasovan, I. Towers, A. V. Buryak, B. A. Malomed, L. Torner, J. P. Torres, and F. Lederer, Phys. Rev. Lett. **88**, 073902 (2002).

[17] D. Mihalache, D. Mazilu, F. Lederer, Y. V. Kartashov, L.-C. Crasovan, L. Torner, and B. A. Malomed, Phys. Rev. Lett. **97**, 073904 (2006).

[18] J. Hukriede, D. Runde, and D. Kip, J. Phys. D **36**, R1 (2003).

[19] B. A. Malomed, *Soliton Management in Periodic Systems* (Springer: New York, 2006).

[20] P. G. Kevrekidis, G. Theocharis, D. J. Frantzeskakis, and Boris A. Malomed, Phys. Rev. Lett. **90**, 230401 (2003).

[21] K. M. O'Hara, S. L. Hemmer, M. E. Gehm *et al.*, Science **298**, 2179 (2002); H. Xiong, S. Liu, W. Zhang *et al.*, Phys. Rev. Lett. **95**, 120401 (2005).

[22] O. L. Borovkova, Y. V. Kartashov, B. A. Malomed, and L. Torner, Opt. Lett. **36**, 3088 (2011).

[23] M. M. Cerimele, M. L. Chiofalo, F. Pistella, S. Succi, and M. P. Tosi, Phys. Rev. E **62**, 1382 (2000).

[24] W. Bao, I-L. Chern, F. Y. Lim, Journal of Comput. Phys. **219**, 836 (2006); W. Bao and Y.Z. Zhang, Math. Models Meth. Appl. Sci. **15**, 1863 (2005).

[25] D. S. Wang, S. W. Song, B. Xiong, and W. M. Liu, Phys. Rev. A **84**, 053607 (2011).

[26] V. M. Lashkin, A. S. Desyatnikov, E. A. Ostrovskaya, and Y. S. Kivshar, Phys. Rev. A **85**, 013620 (2012).